Proceedings of the 3rd International Conference on Functional Materials and Civil Engineering
DOI: 10.54254/2755-2721/2025.24099

Precise Control of Oxygen Coordination Number in Iron-Phenolic Networks for Enhanced Oxygen Evolution Reaction Catalysis

Jiantong Xu[1*], Hengjia Shao[2]

[1]*Materials and Manufacturing, Beijing University of Technology, Beijing, China*
[2]*Institute of Energy Materials Science, University of Shanghai for Science and Technology, Shanghai, China*
**Corresponding Author. Email: 1114959122@qq.com*

Abstract: The local structure of single metal sites is critical for optimizing catalytic activity, yet their precise control of coordination number remains a significant challenge. This study demonstrates that the coordination environment of iron (Fe) in metal-phenolic networks (MPNs) can be systematically tuned with oxygen coordination numbers of 2, 4, and 6 by adjusting pH during synthesis. Electrochemical tests reveal that Fe-2O exhibits superior oxygen evolution reaction (OER) performance, achieving a low overpotential of 270 mV at 10 mA cm^{-2}, a Tafel slope of 66.82 mV dec^{-1}, and excellent stability over 27 hours. In contrast, Fe-4O and Fe-6O show progressively higher overpotentials and reduced stability, with Fe-6O performing nearly as poorly as bare nickel foam. The low oxygen coordination of Fe can facilitate efficient charge transfer and enhance OER activity. This work highlights the importance of tailoring the coordination environment of single metal sites to optimize catalytic performance.

Keywords: OER Catalysis, Fe-O Coordination, Iron-Phenolic Networks, DFT calculation

1. Introduction

The continuously growing global population, economic expansion, and rapid urbanization have led to a substantial increase in energy demand [1]. Conventional fossil fuels such as petroleum and coal now face depletion crises despite their historical dominance in energy supply [2]. This urgent situation makes the transition to alternative clean, sustainable, and renewable energy sources crucial for achieving decarbonized energy systems, ensuring future energy sustainability and global security [3]. Hydrogen energy, as a superior green energy carrier, has garnered increasing worldwide attention [4-6]. However, the oxygen evolution reaction (OER) requires overcoming an overpotential and involves complex dynamic adsorption/desorption processes of multiple intermediates (e.g., *O, *OOH), imposing stringent requirements on catalyst electronic structures and surface microenvironments [7].

Coordination number (CN), as a key structural parameter, directly influences the geometric configuration and electronic properties of active sites, thereby determining the activation energy of OER rate-determining steps. Jie Zeng designed Ir single atoms with second-shell Ir-O-Ni coordination on NiO supports. At a coordination number of 4, increased dz^2 orbital electron occupation in Ir effectively mitigated excessive *OOH intermediate adsorption, achieving an intrinsic

© 2025 The Authors. This is an open access article distributed under the terms of the Creative Commons Attribution License 4.0 (https://creativecommons.org/licenses/by/4.0/).

DOI: 10.54254/2755-2721/2025.24099

current density of 0.4 mA/cm² at 300 mV overpotential with 2-3-fold activity enhancement [8]. It has also been reported that the CN of Pt single atoms increasing from 2 to 4 can significantly reduce the OER energy barriers [9]. Notably, Yanmei Shi et al. [10] constructed TA-Ni_3Fe composite membranes on carbon fiber paper through coordination modulation of TA with transition metals (Fe, Co, Ni). This catalyst achieved a remarkably low overpotential of 290 mV at 10 mA/cm² with a Tafel slope of 28 mV/dec, outperforming commercial RuO_2. These advances demonstrate that precise regulation of Fe-O coordination environments can effectively optimize metal center electron density and intermediate adsorption strength, opening new avenues for designing high-performance OER catalysts.

Herein, we present a facile strategy for precisely controlling the oxygen coordination number of metal (Fe) -phenolic networks (MPNs). The Fe-phenolic networks demonstrate unique advantages through polyphenol ligands' strong chelation capacity and diverse metal coordination modes. Natural polyphenols like tannic acid (TA), containing abundant catechol groups, enable pH-dependent gradient coordination with Fe^{3+} ions to form stable Fe-O structures [11-12]. Among the three pH-tuned coordination complexes, the sample prepared at pH < 2 (denoted as Fe-2O), 3<pH < 6 (denoted as Fe-4O), and pH > 7 (denoted as Fe-6O). The Fe-2O exhibited optimal OER performance with an overpotential of 270 mV at 10 mA cm^{-2} and a Tafel slope of 66.82 mV dec^{-1}. The experimental and theoretical results confirm that the regulation of oxygen coordination numbers of Fe single metal site is crucial to achieve the outstanding OER performance. It is believed that the changed electronic structure by modulating the local environment of Fe singe metal site facilitates efficient charge transfer and thus, enhances OER activity.

2. Methodology

Nickel foam (NF) substrate pretreatment: NF sheets (1 mm thickness) were cut into 1 × 1.5 cm rectangular pieces. The substrates underwent sequential ultrasonic cleaning in acetone (15 min), deionized water (15 min), and ethanol (15 min) to remove surface impurities, followed by drying under nitrogen flow; Solution preparation: Iron (III) chloride solution: 0.1 g $FeCl_3 \cdot 6H_2O$ (Sigma-Aldrich, 99%) was dissolved in 100 mL deionized water, then diluted to 500 mL in a volumetric flask. Tannic acid (TA) solution: 0.4 g TA (Aladdin, ≥98%) was dissolved in 500 mL deionized water using identical dilution procedures; MPN@NF fabrication: Pretreated NF substrates were immersed in three separate beakers containing 25 mL TA solution each. After thorough stirring, 25 mL $FeCl_3 \cdot 6H_2O$ solution was added to each beaker, yielding deep blue solutions. Subsequent pH adjustments were made using: pH < 2: 0.1 M HCl addition (solution color transitioned to pale blue).pH 5 & 10: 1 M NaOH addition (solution darkened).The NF samples were retrieved, oven-dried at 80°C (12 hr), and subjected to four consecutive coating cycles (immersion-stirring-drying) to complete Fe-MPN@NF synthesis.; MPN powder synthesis: pH-adjusted solutions were flash-frozen at -40°C (2 hr) and lyophilized (Free Zone 2.5 L, Labconco) for 48 hr. The resulting powders were purified via sequential washing with ethanol/water (1:1 v/v) under ultrasonication (30 min) and centrifugation (8,000 rpm, 10 min), collecting the precipitated MPN powders for further characterization.

3. Results and discussions

Atomic-level regulation of metal-ligand coordination architecture critically determines catalytic efficacy, yet challenging. Previous studies have informed that the coordination of oxygen can be accurately shifted from the reaction between tannic acid (TA) and iron chloride hexahydrate under three distinct pH conditions [13]. At pH levels below 2, the solution mainly forms mono-complex of the Fe-O molecules with a coordination number (CN) of 2. When the pH increases to the value

DOI: 10.54254/2755-2721/2025.24099

between 3 and 6, the CN of Fe-O shifts to 4. Further increasing the pH 7, the CN of Fe-O reaches 6. The three samples were named by the coordination numbers, which correspond to the Fe-2O, Fe-4O, and Fe-6O (Figure 1a). The UV-Vis spectra of these solutions, depicted in Figure 1(b), show that as the pH increases, the peak intensity at lower angles also increases, suggesting a redshift in the absorption maximum. This phenomenon is caused by the formation of tris-catechol from bis-catechol. This shift indicates a stronger ligand field, which varies with the Fe^{3+}-TA coordination modes at different pH levels, corroborating the increase in Fe-O coordination numbers. Also, the color of the solution changes upon mixing of alkalines, depending on the pH. As shown in Figure 1c, it appears transparent gray at pH < 2, pale blue at pH = 5, and light red at pH = 10. The Fe-O coordination is facilitated by the dehydroxylation of the catechol groups in TA. Additionally, the resulting metal-phenolic compounds adhere to the nickel foam (NF).

Surface through π-π interactions or chelation [14]. Scanning electron microscopy (SEM) images distinguish between two regions: black flocculent aggregates (composed of stacked Fe-MPN) and white areas, with EDS data supporting these observations (Figure 2). The Cryo-spherical Aberration Corrected Transmission Electron Microscope was employed to analyze the elemental distribution of Fe-2O framework and atomic structure of Fe-2O. The EDS result show that the Fe, O, and C are uniformly distributed over the architecture of Fe-2O networks (Figure 1d, Figure 3). The HRTEM image of Fe-2O networks indicates that there are several bright spots, which correspond to the Fe atoms due to their high reflecting electronic intensity (Figure 1e and f, Figure 4). Interestingly, the Fe atoms have dimer structures, consistent with the Fe-2O molecule design. The X-ray diffraction patterns (XRD) analysis was performed on freeze-dried Fe-MPN powders. The XRD of all three samples exhibit amorphous structures, indicating disordered coordination conducive to active site exposure (Figure 5). The SEM-EDS confirms an uniform C/Fe/O distribution across the selected areas, with O content increasing and Fe content decreasing at higher pH (Figure 6).

Also, the XPS analysis verified the presence of C 1s, O 1s, and Fe 2p in all samples (Figure 7). The high-resolution O 1s spectra displayed two peaks at 531.7 eV (C–O) and 530.2 eV (C–O–Fe), with the latter intensifying at higher pH, reflecting enhanced Fe–O coordination saturation (Figure 8a) [15]. This result indicates the highest ratio of C-O-Fe bonds in the Fe-6O sample, which is consistent with previous analysis. The X-ray adsorption spectra (XAS) is further conducted to further determine the coordination enviro nment of Fe single metal sites in all samples. The Fe2O3 and Fe foil are utilized as reference materials. The X-ray absorption near edge spectra (XANES) results show a pH-dependent increase in oxidation status of Fe (Figure 8b). The Fe-6O has the highest valence while the Fe-2O species indicates the lowest valence.agglomeration of Fe molecules with hydroxides in high pH level. The EXAFS fitting results confirm that the coordination numbers of Fe-2O, Fe-4O, and Fe-6O are 3.2 ± 0.6, 4.8 ± 0.9, and 6.4 ± 1.3, respectively (Table 1, and Figure 8d). Deviations from ideal coordination numbers (2/4/6) may result from Na^+/Cl^- impurities or the presence of high-coordination-number species. Under acidic conditions, hydroxyl bridging was inhibited, favoring low-coordination-number open structures, whereas alkaline conditions promoted multidentate coordination with shortened bonds and electron localization. Wavelet transform analysis provided additional evidence for Fe–O bonding, which shows that the coordination number is increasing with the increase of pH levels (Figure 8e).

DOI: 10.54254/2755-2721/2025.24099

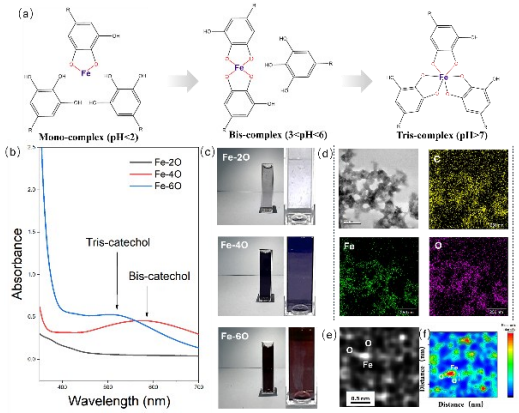


Figure 1: a) The schematic illustration of oxygen coordination regulation of Fe MPNs by adjusting pH levels. b) The UV-Vis spectra of the Fe-2O, Fe-4O, and Fe-6O. c) The solution colors of the Fe-2O, Fe-4O, and Fe-6O. d) The STEM-EDS results of Fe-2O. e) The Fourier reverted HRTEM image of the Fe-2O sample, and f) its corresponding electronic profile

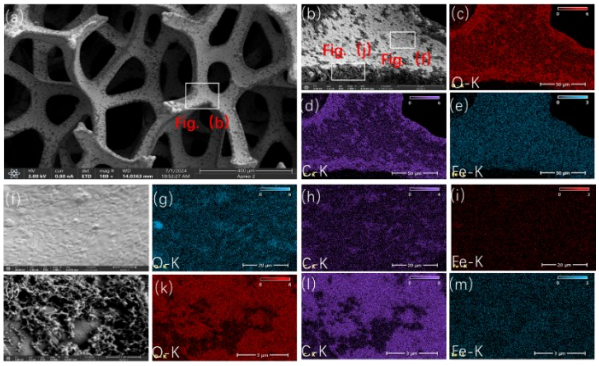


Figure 2: Fe phenolic network loaded on nickel foam (NF) : a) overall SEM; b) Local SEM images after magnification; c) element O distribution; d) element C distribution;e) element Fe distribution; f) SEM images with enlarged white areas in the image; g) element O distribution; h) element C distribution; i) element Fe distribution; j) SEM image with enlarged black area in the image; k) element O distribution; (l) element C distribution; m) element Fe distribution

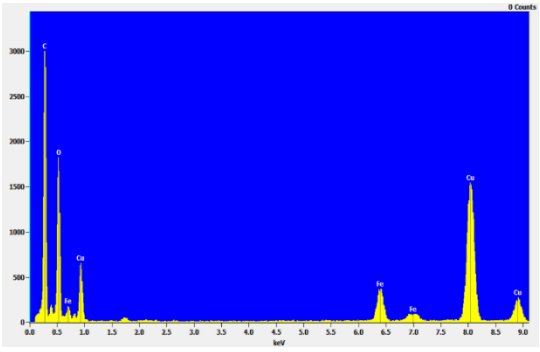


Figure 3: EDS results in TEM images of Fe phenolic networks loaded on copper networks of Fe-2O

DOI: 10.54254/2755-2721/2025.24099

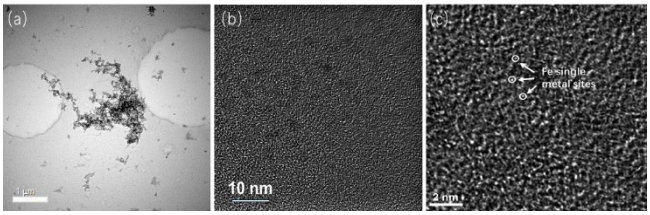


Figure 4: Transmission electron microscopy (TEM) images of Fe phenolic networks loaded on copper networks of Fe-2O: a) TEM images; b) HRTEM images; c) Fourier reverted HRTEM images

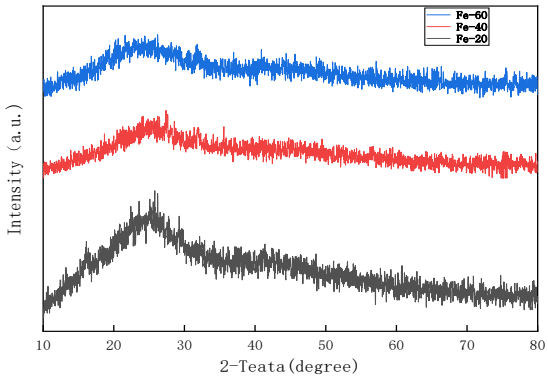


Figure 5: Powder X-ray diffraction (XRD)

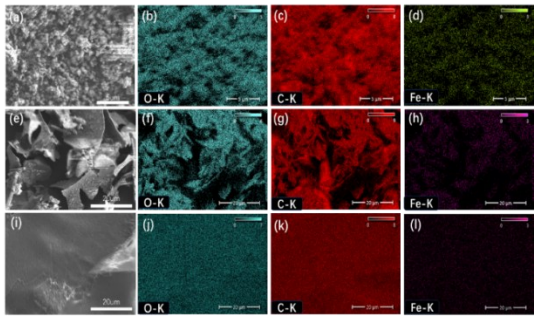


Figure 6: The catalyst powder after Fe metal ion and tannic acid are frozen and dried at three pH values; Fe-2O: (a) SEM image and EDS image of element distribution; (b) element O distribution; (c) element C distribution; (d) element Fe distribution; Fe-4O: (e) SEM image and EDS image of element distribution; (f) element O distribution; (g) element C distribution; (h) element Fe distribution; Fe-6O: (i) SEM image and EDS image of element distribution; (j) element O distribution;(k)element C distribution;(l) element Fe distribution

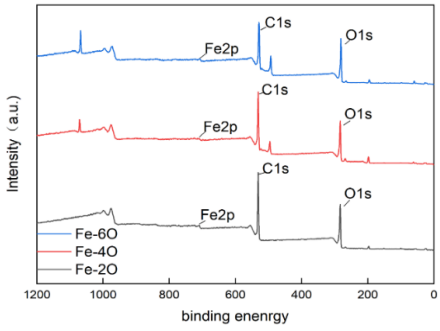


Figure 7: X-ray photoelectron spectroscopy (XPS) of Fe-6O, Fe-4O, and Fe-2O

DOI: 10.54254/2755-2721/2025.24099

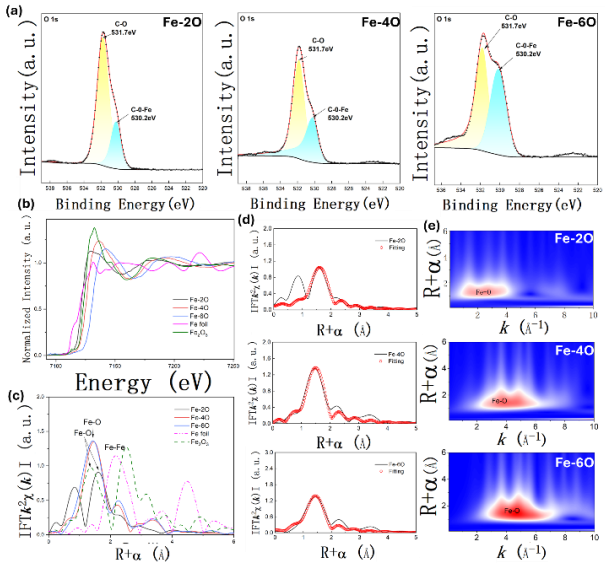


Figure 8: a) X-ray photoelectron spectroscopy (XPS) of TA and O 1s spectra.X-ray absorption spectra of Fe-MPN powder: b) E-space; c) R space; d) R space geometry; e) Wavelet conversion

Tabel 1: EXAFS fitting parameters at the Fe K-edge for various samples

Sample	Shell	CN[a]	R(Å)[b]	σ^2(Å^2)[c]	ΔE_0(eV)[d]	R factor
Fe foil	Fe-Fe	8.0*	2.47±0.01	0.0046	5.9	0.0058
	Fe-Fe	6.0*	2.85±0.01	0.0057		
Fe2O3	Fe-O	6.5±1.3	1.98±0.01	0.0116	-2.9	0.0147
Fe-2	Fe-O	3.2±0.6	2.07±0.01	0.0030	6.0	0.0191
Fe-5	Fe-O	4.8±0.9	1.99±0.01	0.0030	0.0	0.0166
Fe-10	Fe-O	6.4±1.3	1.96±0.01	0.0060	-5.7	0.0055

To demonstrate the effectiveness of our samples, we conducted electrochemical tests to evaluate their performance in the oxygen evolution reaction (OER). The mass loading of all samples is listed in Figure 9. The experiments were carried out in a 1M KOH solution. As illustrated in Figure 10a, the Fe-2O sample exhibits superior OER activity, showing the lowest overpotential of 270 mV to achieve a current density of 10 mA cm^{-2}. In contrast, the OER performance declines as the oxygen coordination number increases. Specifically, Fe-4O and Fe-6O present higher overpotentials of 335 mV and 435 mV, respectively. Notably, the overpotential for Fe-6O is nearly equivalent to that of bare nickel foam (NF), indicating a loss of OER activity when the oxygen coordination number rises to six. To further evaluate efficiency, we calculated Tafel slopes. The slope for Fe-2O is measured at 66.82 mV dec^{-1}, which is lower than those for both Fe-4O and Fe-6O (Figure 10b). This finding suggests that Fe-2O has a faster transformation efficiency compared to its counterparts. Stability is another critical factor for practical energy conversion devices. Our stability tests reveal that Fe-2O can sustain OER performance at low potential without an increase in voltage after 27 hours (Figure 10c). Conversely, both Fe-4O and Fe-6O show increased overpotentials of 40 mV and 100 mV, respectively. When compared to previously reported iron-based OER catalysts, our findings indicate remarkably low overpotential values. These results underscore the significance of oxygen coordination number in modulating OER catalytic activity (Figure 10d).

DOI: 10.54254/2755-2721/2025.24099

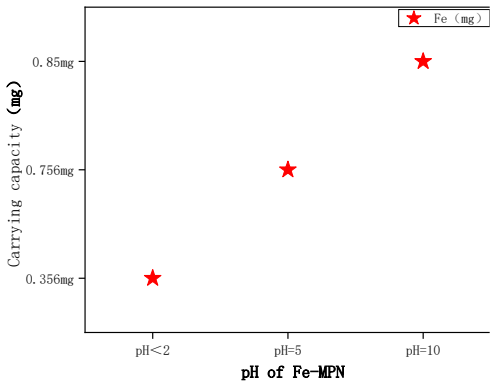


Figure 9: Inductively coupled plasma ICP test results

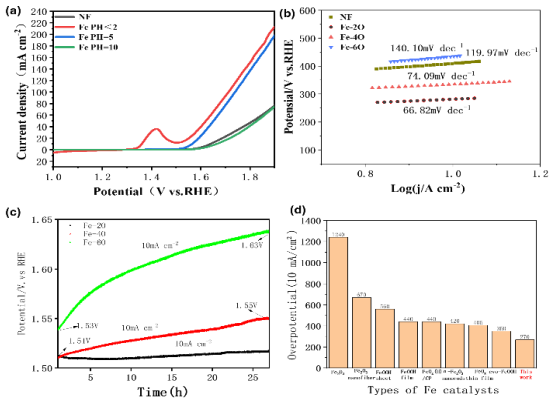


Figure 10: Electrochemical test results of oxygen evolution reaction of Fe metal phenol aldehyde network at three different pH: a) LSV curve; b) Tafel slope curve; c) Electrochemical stability test V-t curve; d) LSV comparison diagram of Fe based oxides

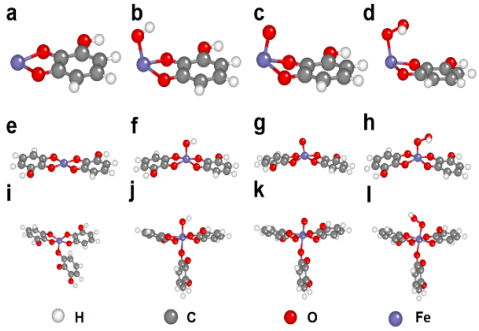


Figure 11: Optimized structures of tannic acid under different pH conditions for key OER intermediates. (a–d) Structures of *, OH*, O*, and OOH* of Fe-2O. (e–h) Structures of *, OH*, O*, and OOH* Fe-4O. (i–l) Structures of *, OH*, O*, and OOH* Fe-6O

DOI: 10.54254/2755-2721/2025.24099

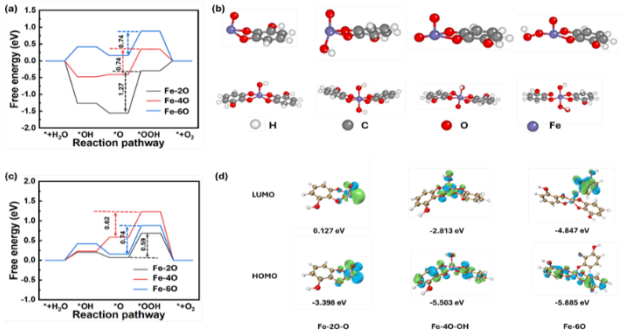


Figure 12: a) Gibbs free energy change diagrams. b) Optimized structures of *, OH*, O*, and OOH* after O adsorption. c) Gibbs free energy change diagrams for Fe-2O after O adsorption, Fe-4O after OH adsorption, and Fe-6O. d) HOMO-LUMO energy levels of tannic acid under different pH conditions: Fe-2O after O adsorption, Fe-4O after OH adsorption, and Fe-6O

Examine the impact of pH on the OER catalytic activity of Fe-MPN, density functional theory (DFT) calculations were performed [16, 17]. Due to the significant structural changes of tannic acid under different oxygen coordination numbers, three models corresponding to CN = 2, 4, and 6 were constructed to simulate their OER process at varying pH levels. The optimized structures of Fe-2O, Fe-4O, and Fe-6O are shown in Figure 11 and the computational details are provided. To evaluate the influence of CN on the OER activity, we calculated the free energy change curves of Fe-2O, Fe-4O, and Fe-6O, as presented in Figure 12a. The results indicate that at Fe-2O and Fe-4O, the adsorption free energies of O* and OH* are relatively low, suggesting stronger binding to oxygen-containing intermediates. In contrast, at Fe-6O, the adsorption free energies of O* and OH* become positive, indicating significantly weaker adsorption capability. This weakened interaction with oxygen intermediates leads to a reduction in overall catalytic performance. Since O and OH adsorption is relatively strong at Fe-2O and Fe-4O, we further optimized the computational models to accurately describe the OER reaction pathway by explicitly including an additional O and OH adsorption site in the Fe-2O and Fe-4O models (Figure 12b). The calculation results reveal that, under all pH conditions, the rate-determining step (RDS) is consistently O* → OOH*, with the corresponding free energy changes of 0.59 eV (Fe-2O), 0.62 eV (Fe-4O), and 0.74 eV (Fe-6O) (Figure 12c). These results indicate that the formation of OOH is the key step determining the OER rate*, and among the studied conditions, Fe-2O exhibits the lowest energy barrier, suggesting the highest catalytic activity. To evaluate the electron-donating and accepting abilities of the material, we calculated the HOMO-LUMO energy levels for Fe-2O, Fe-4O, and Fe-6O, as shown Figure 12d. The HOMO energy level is a key descriptor of the material's electron-donating ability, with a higher HOMO value indicating a greater tendency to donate electrons [18]. The result indicates that the HOMO energy level of Fe-2O is the highest at -3.4 eV, followed by Fe-4O (-5.49 eV) and Fe-6O (-5.88 eV). Fig.13 indicate that Fe-2O exhibits the strongest electron-donating capability, which may facilitate charge transfer and contribute to its enhanced catalytic performance. The results reveal that with increasing Fe–O coordination number, the d-band center (εd) of the three samples gradually shifts away from the Fermi level, with calculated values of −1.24 eV for Fe-2O, −1.42 eV for Fe-4O, and −1.66 eV for Fe-6O (all relative to the Fermi level). This trend indicates that Fe-2O possesses more accessible d-states near the Fermi level, which facilitates electron donation and enhances interaction with oxygen intermediates—consistent with its higher HOMO energy level and superior OER performance.

DOI: 10.54254/2755-2721/2025.24099

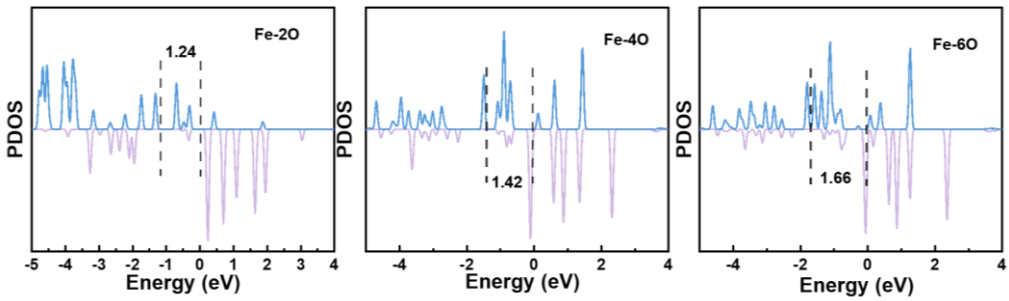


Figure 13: Density of states (PDOS) and d-orbital population analyses to further quantify the ligand field strength

4. Conclusions

The precise control of the coordination number (CN) of single metal sites is crucial for optimizing catalytic activity, particularly in the oxygen evolution reaction (OER). This study demonstrates that the coordination environment of Fe-MPN can be systematically tuned by adjusting the pH during synthesis. At pH < 2, Fe-2O with a CN of 2 forms, while increasing the pH to 3–6 and >7 results in Fe-4O (CN = 4) and Fe-6O (CN = 6), respectively. Fe-2O exhibits the highest catalytic activity, achieving a low overpotential of 270 mV at 10 mA cm^{-2}, a Tafel slope of 66.82 mV dec^{-1}, and excellent stability over 27 hours. In contrast, Fe-4O and Fe-6O show progressively higher overpotentials and reduced stability, with Fe-6O performing nearly as poorly as bare nickel foam. DFT calculations further support these findings, revealing that Fe-2O has the lowest energy barrier (0.59 eV) for the rate-determining step (O* → OOH*) and the strongest electron-donating capability, as indicated by its highest HOMO energy level (-3.4 eV). These properties facilitate efficient charge transfer and enhance OER activity. In summary, this work underscores the importance of tailoring the coordination environment of single metal sites to optimize catalytic performance. By controlling pH during synthesis, it is possible to fine-tune the coordination number and electronic structure of Fe-based catalysts, leading to significant improvements in OER efficiency. These insights provide a valuable framework for designing advanced electrocatalysts for energy conversion applications.

Authorship statement

Jiantong Xu (First Author and Corresponding Author): Conceptualization, Methodology, Investigation, Visualization, Validation, Supervision, Writing-Original Draft, Writing- Review & Editing; Hengjia Shao: Visualization, Writing - Original Draft.

Conflicts of interest

There are no conflicts to declare.

Data availability

The data supporting the findings of this study are available within the article and its ESI.†

Acknowledgments

This work was supported by the National Key R&D Program of China (grant number 2021YFB3500800).

DOI: 10.54254/2755-2721/2025.24099

References

[1] Jie H, Khan I, Alharthi M, et al. Sustainable energy policy, socio-economic development, and ecological footprint: The economic significance of natural resources, population growth, and industrial development[J]. Utilities Policy, 2023, 81: 101490.

[2] Farghali M, Osman A I, Mohamed I M A, et al. Strategies to save energy in the context of the energy crisis: a review[J]. Environmental Chemistry Letters, 2023, 21(4): 2003-2039.

[3] HUI Y, WANG M, GUO S, et al. Comprehensive review of development and applications of hydrogen energy technologies in China for carbon neutrality: technology advances and challenges [J]. Energy Conversion and Management, 2024, 315: 118776.

[4] GRäTZEL M. Photoelectrochemical cells [J]. nature, 2001, 414(6861): 338-44.

[5] COUNCIL A. BULLETIN NO. 6 FEBRUABX 1958 [J].

[6] GIELEN D, BOSHELL F, SAYGIN D, et al. The role of renewable energy in the global energy transformation [J]. Energy strategy reviews, 2019, 24: 38-50.

[7] LAI W H, ZHANG L F, HUA W B, et al. General π-electron-assisted strategy for Ir, Pt, Ru, Pd, Fe, Ni single-atom electrocatalysts with bifunctional active sites for highly efficient water splitting [J]. Angewandte Chemie Internati onal Edition, 2019, 58(34): 11868-73.

[8] WEI J, TANG H, LIU Y, et al. Optimizing the Intermediates Adsorption by Manipulating the Second Coordination Shell of Ir Single Atoms for Efficient Water Oxidation [J]. Angewandte Chemie, 2024, 136(44): e202410520.

[9] KUMARI S, SAUTET P. Highly dispersed Pt atoms and clusters on hydroxylated indium tin oxide: a view from first-principles calculations [J]. Journal of Materials Chemistry A, 2021, 9(28): 15724-33.

[10] SHI Y, YU Y, LIANG Y, et al. In situ electrochemical conversion of an ultrathin tannin nickel iron complex film as an efficient oxygen evolution reaction electrocatalyst [J]. Angewandte Chemie International Edition, 2019, 58(12): 3769-73.

[11] EJIMA H, RICHARDSON J J, LIANG K, et al. One-step assembly of coordination complexes for versatile film and particle engineering [J]. Science, 2013, 341(6142): 154-7.

[12] GUO J, PING Y, EJIMA H, et al. Engineering multifunctional capsules through the assembly of metal–phenolic networks [J]. Angewandte Chemie International Edition, 2014, 53(22): 5546-51.

[13] EJIMA H, RICHARDSON J J, LIANG K, et al. One-step assembly of coordination complexes for versatile film and particle engineering [J]. Science, 2013, 341(6142): 154-7.

[14] WEI J, WANG G, CHEN F, et al. Sol–gel synthesis of metal–phenolic coordination spheres and their derived carbon composites [J]. Angewandte Chemie, 2018, 130(31): 9986-91.

[15] Geng H, Zhong Q Z, Li J, et al. Metal ion-directed functional metal–phenolic materials[J]. Chemical Reviews, 2022, 122(13): 11432-11473.

[16] LIU F, GAO R, SHI C, et al. Avoiding sabatier's limitation on spatially correlated Pt–Mn atomic pair sites for oxygen electroreduction [J]. Journal of the American Chemical Society, 2023, 145(46): 25252-63.

[17] MENG H, WU B, ZHANG D, et al. Optimizing electronic synergy of atomically dispersed dual-metal Ni–N 4 and Fe–N 4 sites with adjacent Fe nanoclusters for high-efficiency oxygen electrocatalysis [J]. Energy & Environmental Science, 2024, 17(2): 704-16.

[18] ZHAI Y, XIE B, ZHENG C, et al. Trace alcohol ether electrolytes with dual-site hydrogen bonds and modulated solvation structures for ultralong-life zinc-ion batteries [J]. Journal of Colloid and Interface Science, 2025, 678: 886-95.